

Softmax-free Linear Transformers

Jiachen Lu, Li Zhang, Junge Zhang, Xiatian Zhu, Hang Xu, Jianfeng Feng

Abstract—Vision transformers (ViTs) have pushed the state-of-the-art for various visual recognition tasks by patch-wise image tokenization followed by stacked self-attention operations. Employing self-attention modules results in a quadratic complexity in both computation and memory usage. Various attempts on approximating the self-attention computation with linear complexity have thus been made in Natural Language Processing. However, an in-depth analysis in this work reveals that they are either theoretically flawed or empirically ineffective for visual recognition. We identify that their limitations are rooted in retaining the *softmax self-attention* during approximations. Specifically, conventional self-attention is computed by normalizing the scaled dot-product between token feature vectors. Preserving the softmax operation challenges any subsequent linearization efforts. Under this insight, a *SOftmax-Free Transformer* (abbreviated as **SOFT**) is proposed for the first time. To eliminate the softmax operator in self-attention, a Gaussian kernel function is adopted to replace the dot-product similarity. This enables a full self-attention matrix to be approximated via a low-rank matrix decomposition. The robustness of our approximation is achieved by calculating its Moore-Penrose inverse using a Newton-Raphson method. Further, an efficient symmetric normalization is introduced on the low-rank self-attention for enhancing model generalizability and transferability. Extensive experiments on ImageNet, COCO and ADE20K show that our SOFT significantly improves the computational efficiency of existing ViT variants. Crucially, with a linear complexity, much longer token sequences are permitted in SOFT, resulting in superior trade-off between accuracy and complexity. Code and models are available at <https://github.com/fudan-zvg/SOFT>.

Index Terms—Transformer, linear complexity, softmax normalization, softmax-free, Gaussian attention.

1 INTRODUCTION

RECENTLY the step change brought by Transformers [10] in natural language processing (NLP) [14], [15] seems to have arrived in vision [6], [7], [16], [17]. Indeed, with less inductive bias in its architecture design than Convolution neural networks (CNNs), pure Vision Transformer (ViT) [6] and its variants have shown to be able to outperform CNNs on various vision tasks [18], [19]. However, there is a bottleneck in any Transformer based model, namely its quadratic complexity in both computation and memory usage. This is intrinsic to the self-attention mechanism: given a sequence of tokens (e.g., words or image patches) as input, the self-attention module iteratively learns the feature representations by relating one token to all other tokens. This results in a quadratic complexity $O(n^2)$ with the token sequence length n in both computation (time) and memory (space) since an $n \times n$ sized attention matrix needs to be computed and saved during inference. This problem is particularly acute in vision: a 2D image after tokenization will produce a far longer sequence than those in NLP even with a moderate spatial resolution. This quadratic complexity thus prevents a ViT model from modeling images at high spatial resolutions, which are often crucial for visual recognition tasks.

A natural solution is to reduce the complexity of self-attention computation via approximation. Indeed, there have been a number of attempts in NLP [11], [12], [13], [20]. For example, [11] takes a naive approach by shortening the length of Key and Value via learnable projections. Such a coarse approximation would inevitably cause performance degradation. In contrast, [13], [21] both leverage the kernel mechanism to approximate softmax

normalization to linearize the computation in self-attention. [20] instead adopts a hashing strategy to selectively compute the most similar pairs. Recently, [12] uses Nyström matrix decomposition to reconstruct the full attention matrix with polynomial iteration for approximating the pseudo-inverse of the landmark matrix. Nonetheless, softmax normalization is simply duplicated across the matrix decomposition process, which is theoretically unsound. We empirically found that none of these methods are effective when applied to vision (see Sec. 4.1).

In this work, we identify that the limitations of existing efficient Transformers are caused by the use of *softmax self-attention*, and for the first time propose a softmax-free Transformer. More specifically, in all existing Transformers (with or without linearization), a softmax normalization is needed on top of scaled dot-product between token feature vectors [10]. Keeping this softmax operation challenges any subsequent linearization efforts. To overcome this obstacle, we introduce a novel *softmax-free self-attention* mechanism, named as **SOFT**, with linear complexity $O(n)$ in both space and time. Specifically, SOFT uses Gaussian kernel to define the similarity (self-attention) function without the need for subsequent softmax normalization. With this softmax-free attention matrix, we further introduce a novel low-rank matrix decomposition algorithm for approximation. The robustness of the approximation is theoretically guaranteed by employing a Newton-Raphson method for reliably computing the Moore-Penrose inverse of the matrix.

We make the following **contributions**. **(I)** We introduce a novel *softmax-free Transformer* with linear space and time complexity. **(II)** Our attention matrix approximation is achieved through a novel matrix decomposition algorithm with theoretical guarantee. **(III)** To evaluate our method for visual recognition tasks, we design a family of generic backbone architectures with varying capacities using SOFT as the core self-attention component. Extensive experiments show that with a linear complexity (Figure 1b), our SOFT models can take in as input much longer image token sequences. As a

• *Jiachen Lu and Li Zhang are with the School of Data Science, Fudan University. Junge Zhang is with the School of Mathematical Sciences, Fudan University. Xiatian Zhu is with the Surrey Institute for People-Centred Artificial Intelligence, and Centre for Vision, Speech and Signal Processing (CVSSP), University of Surrey. Hang Xu is with the Huawei Noah Ark Lab. Jianfeng Feng is with the Institute of Science and Technology for Brain-Inspired Intelligence, Fudan University.*

• *Li Zhang is the corresponding author. E-mail: lizhangfd@fudan.edu.cn.*

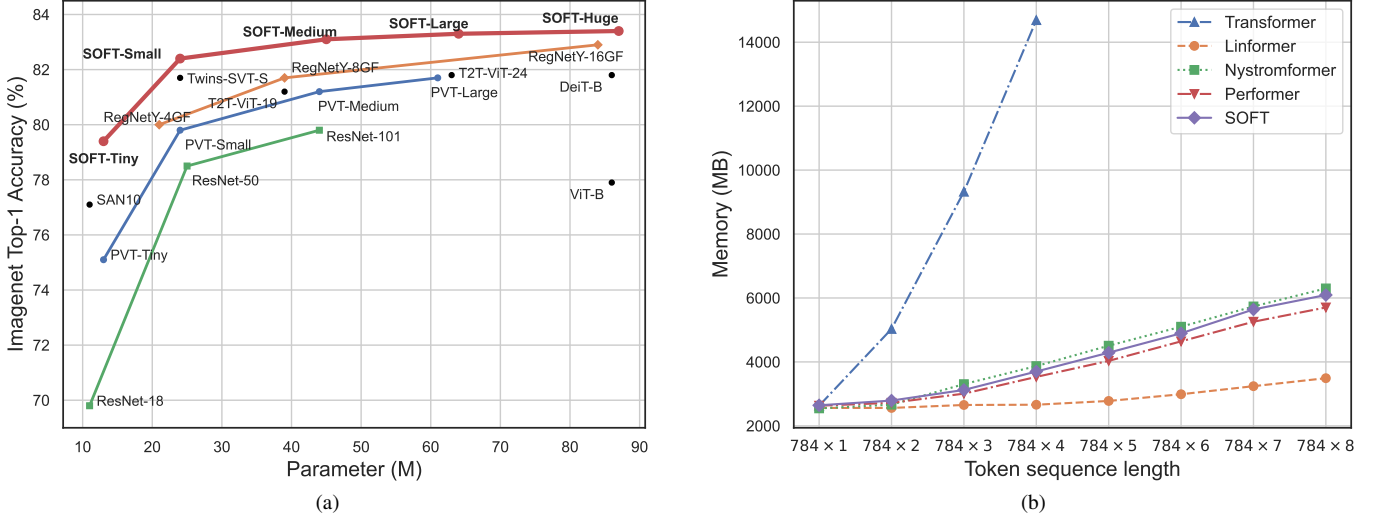


Fig. 1. Top-1 classification accuracy on ImageNet [1] validation set with respect to parameters and the memory usage corresponding to the token sequence length in practice compared to other methods. (a) Comparison with CNN models: RegNet [2], ResNet [3] and Transformer models: PVT [4], DeiT [5], ViT [6], T2T-ViT [7], Twins-SVT [8] and SAN10 [9]; (b) Comparison with Transformer [10], Linformer [11], Nyströmformer [12] and Performer [13]. The memory usage is measured with a batch size of 1 on a 16GB Tesla V100.

result, with the same model size, our SOFT outperforms the state-of-the-art CNNs and ViT variants on ImageNet [1] classification in the accuracy/complexity trade-off (Figure 1a).

A preliminary version of this work was presented in NeurIPS 2021 spotlight [22]. In this paper, we have further extended our conference version as follows: (i) We reveal the significance of normalization in improving model generalizability in softmax self-attention in a perspective of matrix spectral norm. (ii) We prove that the preliminary SOFT has a second order increment of matrix spectral norm with respect to the matrix size, potentially limit model generalizability. (iii) We propose a normalized softmax-free self-attention keeping its linear complexity but with stronger generalizability, along with both theoretical proof and extensive experiments. (iv) Additional experiments show that our SOFT outperforms the state-of-the-art CNNs and ViTs for object detection on COCO [23] and semantic segmentation on ADE20K [24].

2 RELATED WORK

2.1 Vision Transformers

There is a surge of research interests recently in exploiting Transformers for visual recognition tasks [4], [5], [7], [25], [26], inspired by their remarkable success in NLP [10], [14], [15]. Core to these NLP and vision transformers is the same self-attention mechanism [10] that computes a self-attention matrix by exhaustively comparing token pairs. This means a quadratic complexity with the sequence length in both space and time, which thus limits the scalability of Transformers in dealing with long sequences. This limitation is more serious in vision than NLP. To process an image with at least thousands of pixels, patch-wise tokenization is a must for Transformers to control the computational cost. Given higher resolution images, the patch size also needs to be enlarged proportionally sacrificing the spatial resolution. This limits the capability of Transformers, *e.g.*, learning fine-grained feature representation as required in many visual recognition tasks.

2.2 Linear Transformers

Recently, there have been a number of linear/efficient variants [11], [13], [20], [21], [27], [28], [29] of Transformers in NLP. For example, [11] learns to shrink the length of Key and Value based on a low-rank assumption. [20] adopts a hashing strategy to selective the most similar pairs and only compute attention among them. [13], [21] utilize different kernel functions for approximating softmax-based self-attention matrix. [28] applies random feature mapping on the sequences to approach the original softmax function. [29] decreases the time and memory consumption of the attention matrix by replacing the softmax function with its linear-complexity recurrent alternative. When applied to visual recognition tasks, however, we show that these models have considerable performance degradation compared to the standard Transformers [10] (see Sec. 4.1).

The most related work to SOFT is [12] which uses the Nyström matrix decomposition to avoid computing the full attention matrix. However, this method suffers from several theoretical defects: (1) As the standard self-attention needs to apply row-wise softmax normalization on the full attention matrix, a direct application of matrix decomposition is infeasible. As a workaround without solid theoretical support, softmax is simply applied to all the ingredient matrices in [12]. Such an approximation is not guaranteed theoretically. (2) With a polynomial iteration method, it is not guaranteed that the generalized attention matrix inverse can be computed when the matrix is a nearly singular one in practice. In contrast to all the above methods, in this paper we propose a *softmax-free* self-attention mechanism that facilitates matrix decomposition for complexity minimization with theoretical guarantees.

3 METHOD

3.1 Softmax-free self-attention formulation

A schematic illustration of our model is given in Figure 2. Let's first look at our attention module design. Given a sequence of n tokens $X \in \mathbb{R}^{n \times d}$ with each token represented by a d -dimensional

feature vector, self-attention [10] aims to discover the correlations of all token pairs exhaustively.

Formally, X is first linearly projected into three d_e -dimensional spaces (query, key, and values) as:

$$Q = XW_q \in \mathbb{R}^{n \times d_e}, K = XW_k \in \mathbb{R}^{n \times d_e}, V = XW_v \in \mathbb{R}^{n \times d_e}, \quad (1)$$

where $W_q, W_k, W_v \in \mathbb{R}^{d_e \times d_e}$ are learnable matrices. Self-attention can be expressed in a generic formulation as:

$$y_{i,:} = \sum_{j=1}^n \alpha(Q_{i,:}, K_{j,:}) \odot V_{j,:}, \quad (2)$$

where \odot is the Hadamard product, and $i, j \in \{1, \dots, n\}$ index the tokens. The key self-attention function $\alpha : \mathbb{R}^{d_e} \times \mathbb{R}^{d_e} \rightarrow \mathbb{R}$ is composed of a nonlinear function $\beta : \mathbb{R} \rightarrow \mathbb{R}$ and a relation function $\gamma : \mathbb{R}^{d_e} \times \mathbb{R}^{d_e} \rightarrow \mathbb{R}$. A dominant instantiation of α is the scaled dot-product based softmax self-attention [10], defined as

$$\beta(\cdot) = \text{softmax}(\cdot), \quad \gamma(Q_{i,:}, K_{j,:}) = \frac{1}{\sqrt{d_e}} \cdot Q_{i,:}^\top K_{j,:}. \quad (3)$$

Whilst this softmax self-attention has been the *de facto* choice and seldomly questioned, as discussed earlier it is not necessarily suited for linearization. To facilitate the design of linear self-attention, we introduce a softmax-free self-attention function with the dot-product replaced by a Gaussian kernel as:

$$\beta'(\cdot) = \exp(\cdot), \quad \gamma'(Q_{i,:}, K_{j,:}) = -\frac{1}{2\sqrt{d_e}} \cdot \|Q_{i,:} - K_{j,:}\|_2^2. \quad (4)$$

To preserve the symmetric property of attention matrix as in Eq (3), we set the project matrices W_q and W_k in Eq (1) identical (*i.e.*, $Q = K$). Our self-attention matrix is then written as:

$$S_{i,j} = \exp\left(-\frac{1}{2\sqrt{d_e}} \cdot \|Q_{i,:} - K_{j,:}\|_2^2\right). \quad (5)$$

For notation simplicity, we define the matrix formulation as: $S = \exp(Q \ominus K)$.

Remarks: Our self-attention matrix S has three important properties: (1) It is symmetric; (2) All the elements lie in a unit range of $[0, 1]$; (3) All diagonal elements hold the largest value 1 (self-reinforced), with the bottom ones (corresponding to most dissimilar token pairs) being close to 0. As Gaussian kernel is a positive definite kernel [30], S is deemed a Gram matrix. However, we find that when using our kernel-based self-attention matrix S without linearization, the training of a transformer fails to converge. More discussion can be found in Section 3.3.

3.2 Low-rank regularization via matrix decomposition with linear complexity

To solve the convergence and quadratic complexity problems, we leverage matrix decomposition as a unified solution with low-rank regularization. In particular, we consider Nyström [31], which is originally a low-rank matrix approximation algorithm. This enables our model's complexity to be reduced significantly without computing the full self-attention matrix S .

We make this choice because our S is positive semi-definite (*i.e.*, a Gram matrix) without follow-up normalization which are all necessary conditions for Nyström. In contrast, [12] totally ignores these requirements, leading to theoretical flaw in its approximation.

To define the Nyström method formally, let us express $S = \exp(Q \ominus K)$ as a block matrix:

$$S = \begin{bmatrix} A & B \\ B^\top & C \end{bmatrix} \in \mathbb{R}^{n \times n}, \quad (6)$$

where $A \in \mathbb{R}^{m \times m}$, $B \in \mathbb{R}^{m \times (n-m)}$, $C \in \mathbb{R}^{(n-m) \times (n-m)}$ with $m \ll n$. Through Nyström decomposition (see derivative details in Appendix A), an approximation can be represented as:

$$\hat{S} = \begin{bmatrix} A \\ B^\top \end{bmatrix} A^\dagger [A \ B] = P^\top A^\dagger P, \quad \text{where } P = [A \ B], \quad (7)$$

and A^\dagger is the Moore-Penrose (a generalized) inverse of A .

Algorithm 1: SOFT: Softmax-free attention

Input: $Q \in \mathbb{R}^{n \times d_e}$, sampling function f_s
Sampling $\tilde{Q} \leftarrow f_s(Q)$;
 $A \leftarrow \exp(\tilde{Q} \ominus \tilde{Q})$, $P \leftarrow \exp(\tilde{Q} \ominus Q)$;
 $\hat{S} \leftarrow P^\top \text{NR}(A)P$;
Output: \hat{S}

Algorithm 2: NR: Newton-Raphson iteration

Input: $A \in \mathbb{R}^{m \times m}$, and $\mathcal{T} \in \mathbb{Z}^+$
 $\alpha = 2/\|A\|^2$. Initialize $A_0 \leftarrow \alpha A$;
for k from 1 to \mathcal{T} **do**
| $A_k \leftarrow 2A_{k-1} - A_{k-1}AA_{k-1}$
end
Output: $A_{\mathcal{T}}$

Sampling: In the standard Nyström formulation, A and B are sub-matrices of S obtained by randomly sampled m tokens, denoted as \tilde{Q} . We call the sampled \tilde{Q} as *bottleneck tokens*. However, we find empirically that random sampling is considerably sensitive to the choice of m . We hence explore two additional options to leverage the structural prior of visual data: (1) Using one convolutional layer with kernel size k and stride k to learn \tilde{Q} , and (2) Using average pooling with kernel size k and stride k to generate \tilde{Q} . For both, we need to reshape Q to the form of $\mathbb{R}^{H \times W \times d_e}$. Each slide of convolution or pooling produces a token. We set k according to the length of Q such that m tokens can be obtained. Our experiments show that a convolution layer performs better in accuracy. We therefore use a convolution layer by default.

As K is identical to Q , we have $\tilde{K} = \tilde{Q}$. Given these m tokens, we then compute *bottleneck attention* A and P as:

$$A = \exp(\tilde{Q} \ominus \tilde{K}), \quad P = \exp(\tilde{Q} \ominus K). \quad (8)$$

We finally obtain a regularized self-attention matrix \hat{S} of SOFT as:

$$\hat{S} = \exp(Q \ominus \tilde{K}) \left(\exp(\tilde{Q} \ominus \tilde{K}) \right)^\dagger \exp(\tilde{Q} \ominus K). \quad (9)$$

The overall SOFT is summarized in Algorithm 1. The *low-rank* regularization is conducted as follows. For computing the attention score between any two tokens, we first correlate each of them with sampled tokens using our self-attention function (Equation (5)); With this correlation representation we then compute their similarity under the modulation of the generalized inverse of \tilde{Q} 's correlation matrix. Similar as the standard Nyström, our design associates the input tokens w.r.t. a small space spanned by a set of sampled tokens, giving a proper estimation of the original attention relationships subject to a low-rank constraint. This method is proved in Appendix A.

Moore-Penrose inverse: An accurate and commonly used way to calculate the Moore-Penrose inverse is to use Singular Value

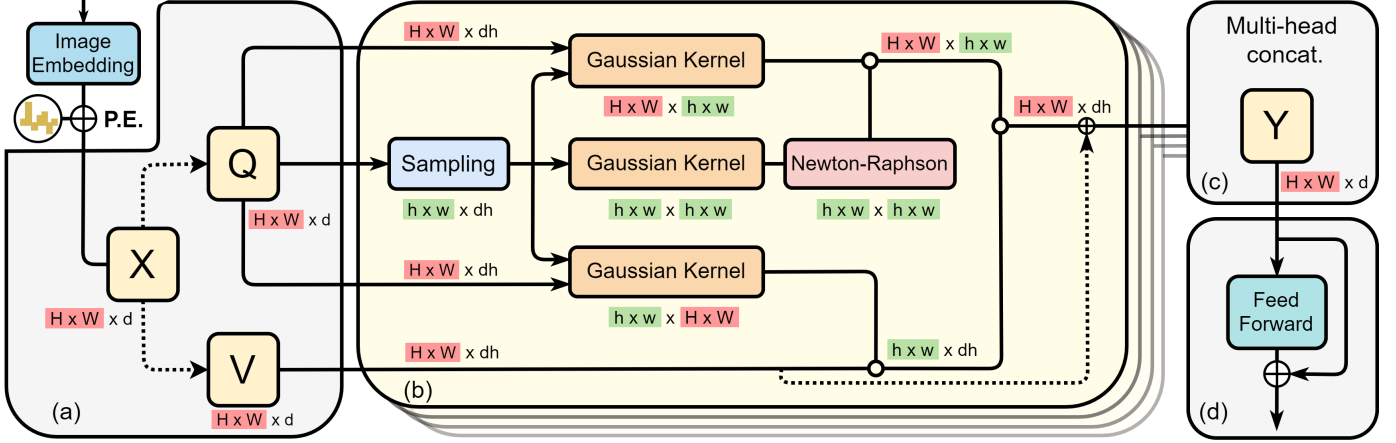


Fig. 2. Schematic illustration of the proposed softmax-free self-attention (SOFT) method. P.E.: Position embedding. Dash lines: linear projection. dh: the hidden dim of each attention head. \circ denotes the matrix dot product.

Decomposition (SVD). Given $A \in \mathbb{R}^{m \times m}$ and its SVD form $A = U\Sigma V^\top$ where U, V are $m \times m$ unitary matrices and Σ is a $m \times m$ diagonal matrix, the Moore-Penrose inverse of A is $A^\dagger = V\Sigma^\dagger U^\top$. Nevertheless, SVD is not friendly to the training process on GPU hence harming the model training efficiency. To solve this issue, we adopt the Newton-Raphson method. It is an iterative algorithm with the $(k+1)$ -th iteration formulated given the previous iteration as:

$$A_{k+1} = 2A_k - A_k A A_k, \quad \text{and} \quad A_0 = \alpha A. \quad (10)$$

We now prove that A_k finally converges to Moore-Penrose inverse of $A_{m \times m}$, if α is sufficiently small [32].

Proposition 1. When α is sufficiently small, $A_{k+1} = 2A_k - A_k A A_k$, A_k converges to A^\dagger .

Proof 1.1. A is a symmetric positive semi-definite matrix and $A_{ij} \leq 1$, $\forall 1 \leq i, j \leq n$, $A_{ii} = 1$, $1 \leq i \leq n$ in our case. A_0 is chosen to be αA , so the A_k can be written as $A_k = C_k A = A D_k$ for some matrix C_k, D_k , leading to the fact that

$$A^\dagger A A_k = A_k, \quad A_k A A^\dagger = A_k. \quad (11)$$

This is because $A_{k+1} = A_k(2I_n - A A_k) = (2I_n - A_k A)A_k$ and $A_0 = \alpha A$. We make a difference between A^\dagger and A_{k+1} :

$$\begin{aligned} A^\dagger - A_{k+1} &= A^\dagger - 2A_k + A_k A A_k \\ &= A^\dagger - A_k A A^\dagger - A^\dagger A A_k + A_k A A_k \\ &= (A^\dagger - A_k)A(A^\dagger - A_k). \end{aligned} \quad (12)$$

We norm both sides of the equation above:

$$\begin{aligned} \|A^\dagger - A_{k+1}\| &= \|(A^\dagger - A_k)A(A^\dagger - A_k)\| \\ &\leq \|A^\dagger - A_k\| \|A(A^\dagger - A_k)\|. \end{aligned} \quad (13)$$

And we left multiply A on the both sides of (Eq 12), then norm the equation:

$$\begin{aligned} \|A A^\dagger - A A_{k+1}\| &= \|A(A^\dagger - A_k)A(A^\dagger - A_k)\| \\ &\leq \|A A^\dagger - A A_k\|^2. \end{aligned} \quad (14)$$

We choose α sufficiently small so that the initial value satisfy $\|A A^\dagger - A A_0\| < 1$. We set $\alpha = \frac{2}{\|A\|_1^2}$ to ensure it is small

enough [32]. Then the $\|A A^\dagger - A A_k\| \rightarrow 0$, when $k \rightarrow \infty$. The inequality (13) implies that $A_k \rightarrow A^\dagger$, $k \rightarrow \infty$.

Though $\alpha = 2/\|A\|_1^2$ which ensures good convergence behavior in Algorithm 2, in practice, we find that using an alternative form gives more stable training and faster convergence. Specifically, in $\|I - A \frac{2\beta^n}{\|A\|_1^2}\|_1 \leq 1$ where β equals to 0.5, we find the smallest n_i that holds this inequality. Then, we initialize α as $\alpha = \frac{2\beta^{n_i}}{\|A\|_1^2}$.

The following proposition comes with the proof of Proposition 1:

Proposition 2. $\|A A_k A - A\|$ and $\|A_k - A^\dagger\|$ decreases to 0 monotonously, if α is sufficiently small.

Proof 2.1. Note that when we multiply A on both sides of (12), the equation turns to be:

$$\begin{aligned} A - A A_{k+1} A &= A(A^\dagger - A_k)A(A^\dagger - A_k)A \\ &= (A A^\dagger - A A_k)(A - A A_k A). \end{aligned} \quad (15)$$

Similarly norm both sides of (15), considering that $\|A A^\dagger - A A_k\| \rightarrow 0$ and $\|A A^\dagger - A A_k\| < 1$ always holds, $\|A - A A_k A\|$ monotonically decreases to 0. The inequality (13) implies that $\|A_k - A^\dagger\|$ decreases to 0 monotonously.

Note that although $\|A - A A_k A\|$ monotonically decreases to 0, $\|A_k A A_k - A_k\|$ cannot be proved to monotonically decrease to 0.

This ensures that our estimated inverse is sufficiently accurate for matrix decomposition, subject to that our SOFT attention is regularized. Besides, in training stage, we find that bottleneck matrix A is always non-singular in practice and its inverse A^{-1} thus exists. Therefore, the iteration can be avoided in back propagation because the differential of matrix inverse can be explicitly expressed as

$$\nabla_x \mathcal{L} = -Y^\top (\nabla_Y \mathcal{L}) Y^\top, \quad (16)$$

where $X \in \mathbb{R}^{m \times m}$ is an non-singular matrix and Y is the inverse of X , i.e. $Y = X^{-1}$, $\nabla_Y \mathcal{L}$ is gradient of loss \mathcal{L} on Y and $\nabla_X \mathcal{L}$ is gradient of loss \mathcal{L} on X .

Proof 2.2. Since $XY = I$, we take derivatives on the both sides

$$\begin{aligned} Y dX + X dY &= 0 \\ dY &= -Y dXY \end{aligned} \quad (17)$$

For loss function \mathcal{L} , we have

$$d\mathcal{L} = \langle \nabla_X \mathcal{L}, dX \rangle = \langle \nabla_Y \mathcal{L}, dY \rangle$$

Recall that the inner product $\langle A, B \rangle = \text{Tr}(A^\top B)$ and $\text{Tr}(ABC) = \text{Tr}(CAB) = \text{Tr}(BCA)$, we have

$$\begin{aligned} \langle \nabla_X \mathcal{L}, dX \rangle &= \langle \nabla_Y \mathcal{L}, dY \rangle \\ &= \langle \nabla_Y \mathcal{L}, -Y dXY \rangle \\ &= -\text{Tr}(\nabla_Y \mathcal{L}^\top Y dXY) \\ &= \langle -Y^\top \nabla_Y \mathcal{L} Y^\top, dX \rangle \end{aligned}$$

Therefore, Eq (16) is proved.

In the setting of Section 4.1, this can accelerate the training throughput from 1730 to 1790 images per second.

Complexity: We summarize the complexity of SOFT in space and time. For *time complexity*, it involves: (1) Sampling: $\mathcal{O}(nd_e)$. (2) Calculating three decomposed matrices: $\mathcal{O}(nmd_e + mnd_e + m^2d_e) = \mathcal{O}(2mnd_e + m^2d_e)$; (3) Moore-Penrose inverse: $\mathcal{O}(\mathcal{T} \times m^3) = \mathcal{O}(\mathcal{T}m^3)$, where \mathcal{T} is the iteration steps. (4) All matrix multiplication: $\mathcal{O}(nm^2 + mnd_e + mnd_e) = \mathcal{O}(nm^2 + 2mnd_e)$. The total time complexity is $\mathcal{O}((d_e + 4mnd_e + m^2)n + \mathcal{T}m^3 + d_e m^2)$. The *space complexity* is decided by four decomposed matrices with $\mathcal{O}(n \times m) + \mathcal{O}(m \times m) + \mathcal{O}(m \times n) + \mathcal{O}(n \times d_e) = \mathcal{O}((2m + d_e)n + m^2)$. As we keep m ($m \ll n$) a fixed constant in our model, both time and space complexity are $\mathcal{O}(n)$, making SOFT a linear self-attention.

3.3 Attention normalization

Model generalizability could be explained in the sense of model's sensitivity against input perturbation. [33] suggests that all parts of a model should have small *spectral norm* (i.e., matrix 2-norm or the largest singular value of a matrix). Concretely, by the triangle inequality $\|XY\|_2 \leq \|X\|_2 \|Y\|_2$ where X and Y are any real matrix, any part with large spectral norm could lead to significant error accumulation. This also applies for self-attention matrix, since it is often symmetric and non-negative definite and its spectral norm corresponds to the largest eigenvalue. We provide more theoretical analysis below. Note that both scale dot-product kernel (linear kernel) and Gaussian kernel are positive definite kernel, so they have non-negative eigenvalues.

Proposition 3. In scaled dot-product based softmax self-attention, assume $\lambda_1 \geq \lambda_2 \geq \dots \geq \lambda_n \geq 0$ are eigenvalues of self-attention matrix $S_{\text{softmax}} \in \mathbb{R}^{n \times n}$, then $\lambda_1 \leq 1$.

Proof 3.1. We rewrite the softmax self-attention as

$$S_{\text{softmax}} = D^{-1}A, \quad (18)$$

where $A \in \mathbb{R}^{n \times n}$ is a real symmetric matrix, and $D = \text{diag}(A\mathbb{1}_n)$. We consider the graph Laplacian L of matrix A defined by $L = D - A$, then the normalized graph Laplacian can be expressed as

$$L_{rw} = D^{-1}L = D^{-1}(D - A) = I - D^{-1}A, \quad (19)$$

where, I is an identity matrix. According to [34], L_{rw} is a real semi-definite matrix, so all the eigenvalue of L_{rw} is non-negative. Therefore, eigenvalues of $I - D^{-1}A$ are non-negative, which leads to the fact that eigenvalues $\lambda_1, \dots, \lambda_n$ of $D^{-1}A$ is less or equal to 1.

This proposition means that softmax normalization is useful in restricting the range of self-attention matrix's eigenvalues to $[0, 1]$

and eventually the effect of error accumulation. This is an important role *softmax* operation plays in improving generalizability with standard self-attention. In contrast, this is not the case for our softmax-free self-attention.

Proposition 4. In Gaussian kernel-based self-attention, if $\lambda_1 \geq \lambda_2 \geq \dots \geq \lambda_n \geq 0$ are eigenvalues of self-attention matrix $S_{\text{gaussian}} \in \mathbb{R}^{n \times n}$, then $\lambda_1 \leq n$.

Proof 4.1.

$$\sum_{i=1}^n \lambda_i = \text{Tr}(A) = n,$$

since the diagonal elements of Gaussian kernel-based self-attention is always 1. Therefore, with the fact that all the eigenvalues are positive, we have $\lambda_1 \leq n$.

A larger upper bound of eigenvalue with our proposed self-attention could thus lead to less generalizability, due to a trend of higher error accumulation. Specifically, for softmax-free self-attention matrix, $\hat{S} = P^\top A^\dagger P$, we have

$$\|\hat{S}\|_2 = \|P^\top A^\dagger P\|_2 \leq \|P\|_2^2 \|A^\dagger\|_2. \quad (20)$$

For the bottleneck matrix of softmax-free attention $A \in \mathbb{R}^{m \times m}$, we assume it is k -connected ($k \ll m$), i.e., there are k fields disconnected with each other. This is because a field represents a semantic part of an image and the number is often small.

Proposition 5. Assume the bottleneck matrix of softmax-free attention, $A \in \mathbb{R}^{m \times m}$ is k -connected. If $\lambda_1 \geq \lambda_2 \geq \dots \geq \lambda_m \geq 0$ are eigenvalues of A^\dagger , then $\lambda_1 = \mathcal{O}(m^2)$ and $\|A^\dagger\|_2 = \mathcal{O}(m^2)$.

To prove Proposition 5, we first introduce the following lemmas.

Lemma 5.1. If F is a non-singular and symmetric matrix, then $\|F\|_2 \leq \|F\|_1$.

Proof 5.1. According to the definition of 2-Norm, we have $F^T F z = \mu^2 z$ with $\mu = \|F\|_2$. Therefore, $\mu^2 \|z\|_1 = \|F^T F z\|_2 \leq \|F^T\|_1 \|F\|_1 \|z\|_1 = \|F\|_\infty \|F\|_1 \|z\|_1$. Since A is non-singular and symmetric,

$$\|F\|_2 \leq \sqrt{\|F\|_\infty \|F\|_1} = \|F\|_1 \quad (21)$$

Lemma 5.2. If F is a real matrix and $\|F\|_p < 1$, then

$$(I - F)^{-1} = \sum_{k=0}^{\infty} F^k \quad (22)$$

with

$$\|(I - F)^{-1}\|_p \leq \frac{1}{1 - \|F\|_p} \quad (23)$$

Proof 5.2.

$$\left(\sum_{k=0}^N F^k \right) (I - F) = I - F^{N+1}$$

Since $\|F\|_p < 1$, $\lim_{k \rightarrow \infty} F^k = 0$. Thus,

$$\left(\lim_{N \rightarrow \infty} \sum_{k=0}^N F^k \right) (I - F) = I$$

Multiply the equation by $(I - F)^{-1}$ we obtain Eq (22). From that, we can easily get

$$\|(I - F)^{-1}\|_p \leq \sum_{k=0}^{\infty} \|F\|_p^k = \frac{1}{1 - \|F\|_p}$$

TABLE 1

Comparison of different linear/efficient transformer variants on ImageNet [1], based on our multi-stage Tiny configuration (see Table 2). The memory usage is measured with the batch size of 1024 which is our standard training setting. Transformer is tested at a batch size of 256, which is the maximal number possible with the GPU resource at our disposal. Throughput is in format as Train throughput / inference throughput.

Methods	Complexity	Memory	Params	FLOPs	Throughput (img/s)	Top-1 %
Transformer [10]	$\mathcal{O}(n^2)$	19.0GB†	13M	3.9G	1073 / 3240	79.1
Linformer [11]	$\mathcal{O}(n)$	11.7GB	13M	1.9G	2767 / 3779	78.2
Performer [13]	$\mathcal{O}(n)$	15.0GB	13M	2.2G	2037 / 3657	76.1
Nyströmformer [12]	$\mathcal{O}(n)$	17.2GB	13M	2.0G	1891 / 3518	78.6
SOFT	$\mathcal{O}(n)$	15.8GB	13M	1.9G	1730 / 3436	79.4

Now we begin to prove Proposition 5.

Proof 5.3. Since the bottleneck matrix softmax-free attention $\|A\|_1$ is not less than 1, we normalize the matrix as $A_n = D^{-1}A$, where $D = \text{diag}(A\mathbb{1}_m)$. From Lemma 5.2, it follows that

$$\|A_n^{-1}\|_1 \leq \frac{1}{1 - \|1 - A_n\|_1}$$

Since we assume the bottleneck matrix is k-connected, and $k \ll m$,

$$\|1 - A_n\|_1 \leq \frac{(m - k)}{m}$$

Then,

$$\|A_n^{-1}\|_1 \leq \frac{1}{1 - \frac{(m-k)}{m}} = \frac{m}{k} = \mathcal{O}(m)$$

Note that we $D = \mathcal{O}(m)$ by assumption that the bottleneck matrix is k-connected, it follows that

$$\|A^{-1}\|_1 = \|A_n^{-1}D\|_1 \leq \|A_n^{-1}\|_1\|D\|_1 = \mathcal{O}(m^2)$$

This proposition indicates that $\|\hat{S}\|_2$ is proportional quadratically with the length m of bottleneck token sequence. It implies that the above SOFT formula would be limited to the applications with short bottleneck token sequences (e.g., image classification).

Proposition 6. For the bottleneck matrix of SOFT self-attention $A \in \mathbb{R}^{m \times m}$, we have

$$\|D^{-1/2}A^\dagger D^{-1/2}\|_2 = \mathcal{O}(m), \quad (24)$$

where $D = \text{diag}(A\mathbb{1}_m)$ and $\mathbb{1}_m$ is an all one m -D vector.

Proof 6.1.

$$\|D^{-1/2}A^\dagger D^{-1/2}\|_2 \leq \|D^{-1/2}\|_2^2\|A^\dagger\|_2 = \|D^{-1}\|_2\|A^\dagger\|_2,$$

also, D is a diagonal matrix,

$$\|D^{-1}\|_2\|A^\dagger\|_2 = \|D^{-1}A^\dagger\|_2 = \|A_n^\dagger\|_2^2 = \mathcal{O}(m)$$

This proposition suggests that symmetric normalization can lower the largest eigenvalue of A^\dagger , reducing the spectral norm of \hat{S} .

Attention normalization: In light of the above theorem, we further introduce normalization in SOFT by the following formulation:

$$\hat{S} = \exp(Q \ominus \tilde{K}) D^{-\frac{1}{2}} \left(\exp(\tilde{Q} \ominus \tilde{K}) \right)^\dagger D^{-\frac{1}{2}} \exp(\tilde{Q} \ominus K), \quad (25)$$

where $D = \text{diag}(\exp(\tilde{Q} \ominus \tilde{K})\mathbb{1}_m)$. This yields a tiny increase of $\mathcal{O}(m^2)$ in the computational complexity, which can be further reduced to $\mathcal{O}(\log m)$ on GPU by parallel reduction algorithm [35]. This unlocks the potential of SOFT for more applications especially those with a need for dense information reasoning (e.g., object detection and semantic segmentation).

3.4 Instantiations

Figure 2 shows how our proposed *softmax-free self-attention* block (**SOFT block**) can be implemented in a neural network. We replace the self-attention block with our SOFT block in the traditional Transformer, that is, we stack a SOFT block with a feed forward residual block [6] to form a *softmax-free Transformer* layer (**SOFT layer**).

Focusing on the general image recognition tasks, we integrate our SOFT layer into the recent pyramidal Transformer architecture [4] to form our final model **SOFT**. Further, several improvements are introduced in patch embedding (*i.e.*, tokenization). Specifically, unlike [4] that uses a combination of non-overlapping convolution and layer normalization [36], we adopt a stack of overlapping convolutions, batch normalization [37] and ReLU non-linearity. Concretely, the STEM is implemented by 3 units of 3x3 Conv→BN→ReLU, with the stride of 2, 1, 2 respectively. Then, one such unit is applied to each of three following down-sampling operations with stride of 2 in the multi-stage architecture.

The architecture hyper-parameters of SOFT are: d : the input channel dimension of SOFT layer. d_e : the embedding dimension of tokens in SOFT block. In practice, we set $d_e = d$. h : the head number of SOFT block. d_h : the channel dimension of each head and $d_h = d_e/h$. n : the input token sequence length of a SOFT block. m : the bottleneck token sequence length of SOFT block. sp : the sampling ratio of token sequence length sampling, which is the ratio between input token sequence length and the bottleneck token sequence length. e : the expansion ratio of the 2-layer feed forward block. In SOFT, for all the stages we set $d_h = 32$, $e = 4$ and $m = 49$, sp varies in each stage according to the input token sequence length. Table 2 details the family of our SOFT configurations with varying capacities (depth and width).

4 EXPERIMENTS

4.1 Image classification

Dataset: We evaluate the proposed SOFT on the ILSVRC-2012 ImageNet-1K dataset [1] with 1.28M training images and 50K validation images from 1,000 classes. Following the common practice, we train a model on the training set and evaluate on the validation set.

Metrics: For model performance, the top-1 accuracy on a single crop is reported. To assess the cost-effectiveness, we also report the model size and floating point operations (*i.e.*, FLOPs).

Implementation details: We use the code base [46] with the default setting to train and test all the models. Specifically, we use weight decay of 0.05 and 10 epochs of linear warm-up. We conduct 300 epochs training with an AdamW optimizer and decreasing

TABLE 2

Architecture specifications of SOFT variants. *sp.*: sampling ratio. *-d*: the hidden dimension. *-h*: the number of heads in the self-attention block. *C33-BN-ReLU*: three 3x3 Conv-BN-ReLU, with the stride of 2, 1, 2 respectively. *C31-BN-ReLU*: one 3x3 Conv-BN-ReLU, with a stride of 2.

	Tiny		Small		Medium		Large		Huge	
C33-BN-ReLU, 64-d										
Stage 1	sp. 8x8, 64-d, 2-h	x 1	sp. 8x8, 64-d, 2-h	x 1	sp. 8x8, 64-d, 2-h	x 1	sp. 8x8, 64-d, 2-h	x 1	sp. 8x8, 64-d, 2-h	x 1
C31-BN-ReLU, 128-d										
Stage 2	sp. 4x4, 128-d, 4-h	x 2	sp. 4x4, 128-d, 4-h	x 3	sp. 4x4, 128-d, 4-h	x 3	sp. 4x4, 128-d, 4-h	x 3	sp. 4x4, 128-d, 4-h	x 5
C31-BN-ReLU, 320-d or 288-d										
Stage 3	sp. 2x2, 320-d, 10-h	x 3	sp. 2x2, 320-d, 10-h	x 7	sp. 2x2, 288-d, 9-h	x 29	sp. 2x2, 320-d, 10-h	x 40	sp. 2x2, 352-d, 11-h	x 49
C31-BN-ReLU, 512-d										
Stage 4 w. cls token	sp. 1x1, 512-d, 16-h	x 2	sp. 1x1, 512-d, 16-h	x 4	sp. 1x1, 512-d, 16-h	x 5	sp. 1x1, 512-d, 16-h	x 5	sp. 1x1, 512-d, 16-h	x 5

TABLE 3

Evaluation results on ILSVRC-2012 ImageNet-1K [1] validation set. We report the results using the input size of 224x224 pixels center cropped from resized images with 256x256 pixels. M.S. Out. stands for whether the model is designed for multi-scale output. \dagger : Corrected FLOPs by taking into account the cost of attention matrix multiplication overlooked in the origin paper.

Model	Style	Resolution	M.S. Out.?	Params	FLOPs	Top-1 %.
ResNet-18 [3]	ConvNets	224 ²	✓	11M	1.9G	69.8
PVT-Tiny [4]	Transformers	224 ²	✓	13M	1.9G \dagger	75.1
Coat-Lite Mini [38]	Transformers	224 ²	✓	11M	2.0G	78.9
LambdaNets-50 [39]	Transformers	224 ²	✓	16M	-	78.9
SOFT-Tiny	SOFT	224 ²	✓	13M	1.9G	79.4
ResNet-50 [3]	Convolution	224 ²	✓	25M	4.1G	78.5
PVT-Small [4]	Transformer	224 ²	✓	24M	4.0G \dagger	79.8
Deit-Small [5]	Transformer	224 ²	✗	22M	4.6G	79.9
T2T-ViT _t -14 [7]	Transformer	224 ²	✗	21M	5.2G	80.7
CPVT-Small [40]	Transformer	224 ²	✓	22M	-	79.9
Swin-T [41]	Transformer	224 ²	✓	29M	4.5G	81.3
Twins-SVT-S [8]	Hybrid	224 ²	✓	24M	3.7G	81.7
SOFT-Small	SOFT	224 ²	✓	24M	3.3G	82.4
ResNet-101 [3]	Convolution	224 ²	✓	44M	7.9G	79.8
PVT-Medium [4]	Transformer	224 ²	✓	44M	7.0G \dagger	81.2
ViT-Small/16 [6]	Transformer	224 ²	✗	48M	9.9G	80.8
Swin-S [41]	Transformer	224 ²	✓	50M	8.7G	83.0
SOFT-Medium	SOFT	224 ²	✓	45M	7.2G	83.1
ResNet-152 [3]	Convolution	224 ²	✓	60M	11.6G	80.8
PVT-Large [4]	Transformer	224 ²	✓	61M	10.1G \dagger	81.7
T2T-ViT _t -24 [7]	Transformer	224 ²	✗	64M	13.2G	82.2
BoTNet-S1-110 [42]	Hybrid	224 ²	✓	55M	-	82.8
SOFT-Large	SOFT	224 ²	✓	64M	11.0G	83.3
CaiT-S36 [43]	Transformer	224 ²	✓	88M	13.9G	83.3
Swin-B [41]	Transformer	224 ²	✓	88M	15.4G	83.3
Twins-SVT-L [8]	Hybrid	224 ²	✓	99M	14.8G	83.3
SOFT-Huge	SOFT	224 ²	✓	87M	16.3G	83.4

learning rate with the cosine annealing schedule. During training, random flipping, mixup [47] and cutmix [48] are adopted for data augmentation. Label smoothing [49] is used for loss calculation. All our variants are trained with a batch size of 1024 on 32G NVIDIA V100 GPUs. We also implement our method using the Mindspore [50].

Comparison with existing linear Transformers: We compare our method with three existing linear Transformer models: Linformer [11], Performer [13], Nyströmformer [12] in terms of model complexity and accuracy.

Two experimental settings are adopted. Under the first setting, for all methods we use the same Tiny (Table 2) architecture for a fair comparison. That is, we replace the core self-attention block in SOFT with each baseline's own attention block with the rest of the architecture unchanged. Note that the *spatial reduction* module of [4] is a special case of Linformer [11]. We set the reduction ratio to be identical to ours. With the same uniform sampling idea, we replace the 1D window averaging of Nyströmformer [12] (for NLP tasks) with 2D average pooling (for images). The downsampling ratio remains identical to ours. It is also worth mentioning that there

TABLE 4

Object detection (RetinaNet [44]) and instance segmentation (Mask R-CNN [45]) results on COCO [23] val2007. We report the results by training 12 epoch (1×) schedule. #P stands for parameter size. AP^b and AP^m represents bounding box AP and mask AP respectively.

Backbone	RetinaNet 1×						Mask R-CNN 1×							
	#P	AP	AP ₅₀	AP ₇₅	AP _S	AP _M	AP _L	#P	AP ^b	AP ^b ₅₀	AP ^b ₇₅	AP ^m	AP ^m ₅₀	AP ^m ₇₅
ResNet18 [3]	21M	31.8	49.6	33.6	16.3	34.3	43.2	31M	34.0	54.0	36.7	31.2	51.0	32.7
PVT-Tiny [4]	23M	36.7	56.9	38.9	22.6	38.8	50.0	33M	36.7	59.2	39.3	35.1	56.7	37.3
SOFT-Tiny	23M	40.0	60.8	42.5	23.7	43.3	53.5	33M	41.2	63.7	44.7	38.2	61.0	41.0
ResNet50 [3]	38M	36.3	55.3	38.6	19.3	40.0	48.8	44M	38.0	58.6	41.4	34.4	55.1	36.7
PVT-Small [4]	34M	40.4	61.3	43.0	25.0	42.9	55.7	44M	40.4	62.9	43.8	37.8	60.1	40.3
Swin-T [41]	38M	41.7	61.2	43.2	26.0	44.3	54.5	48M	42.7	65.2	46.8	39.3	62.2	42.2
SOFT-Small	34M	42.8	63.9	45.7	26.9	46.4	57.6	44M	43.8	66.0	47.5	40.1	63.0	43.0
ResNet101 [3]	57M	38.5	57.8	41.2	21.4	42.6	51.1	63M	40.4	61.1	44.2	36.4	57.7	38.8
PVT-Medium [4]	54M	41.9	63.1	44.3	25.0	44.9	57.6	64M	42.0	64.4	45.6	39.0	61.6	42.1
Swin-S [41]	60M	43.0	63.8	45.7	27.1	46.9	57.2	69M	45.6	67.4	50.0	41.2	64.5	44.3
SOFT-Medium	55M	44.3	64.7	47.4	29.0	48.2	59.9	65M	46.6	67.8	51.2	42.0	64.8	45.2
PVT-Large [4]	71M	42.6	63.7	45.4	25.8	46.0	58.4	81M	42.9	65.0	46.6	39.5	61.9	42.5
SOFT-Large	74M	45.3	66.1	48.7	27.4	49.2	61.4	84M	47.0	68.3	51.7	42.2	65.2	45.4

is no official code released for Reformer [20] and the local Sensitive Hash (LSH) module has strict requirements on the length of input tokens. We thus do not include this method in our comparison.

From Table 3.3 we can make the following observations: (i) Linear Transformer methods substantially reduce the memory and FLOPs while maintain similar parameter size comparing to the Transformer on the Tiny architecture; (ii) Our approach SOFT achieves the best classification accuracy among all the linearization methods. (iii) Our inference speed is on-par with other compared linear Transformers and our training speed is slightly slower than Nystromformer and both are slower than Performer and Linformer. Note that the slow training speed of our model is mostly due to the Newton-Raphson iteration which can only be applied sequentially for ensuring the accuracy of Moore-Penrose inverse. In summary, due to the on-par inference speed we consider the training cost increase is a price worth paying for our superior accuracy.

Under the second setting, we focus on the memory efficiency of SOFT against the baselines. Here we follow the ViT [6] network structure, stacking 12 attention layers with hidden dimension $d = 384$, heads $h = 12$, bottleneck token sequence length $m = 49$. Different attention blocks from the three linearized Transformer variants, Linformer [11], Performer [13], and Nyströmformer [12] are studied. For each Transformer variant, we adjust its token sequence length n in a linear increment. Specifically, we use a token sequence length of $784 \times p$ where $p = 1, 2, 3, 4, 5, 6, 7, 8$ and set batch size 1 to verify whether the memory consumption increases “quadratically” or “linearly”. Figure 1b shows all compared transformer variants including our SOFT indeed have a linear memory usage complexity. This is in contrast with the standard Transformer which cannot cope with long token sequences with a quadratic complexity.

Comparison with state-of-the-art CNNs and ViTs: We compare with state-of-the-art alternatives and report the top-1 accuracy on the ImageNet-1K validation set. FLOPs are calculated at batch size 1. From Figure 1a and Table 3, the following observations are made: (i) Overall, ViT and its variants yield better classification accuracy over CNNs. (ii) We achieve the best performance among the recent pure vision Transformer based methods including ViT [6] and DeiT [5], as well as the state-of-the-art CNN RegNet [2]. (iii) Our SOFT outperforms the most similar (in architecture configuration) Transformer counterparts PVT [4] at all variants. Since the attention module is the main difference, this validates

directly the effectiveness of our model. (iv) We can also beat the latest ViT variants Twins [8] which is designed to address the efficiency limitation of ViT. We have done so with less parameters and fewer float point computation.

To gain some insights into how attention is learned using our SOFT and the alternatives, Figure 3 shows the attention masks of various compared models. For each model, we show the output from the first two attention heads. It is evident that SOFT exhibits robustness and versatility in capturing local and long distance relations among pixels. It is interesting to note that, although SOFT is trained on an object categorization dataset in ImageNet [1], it seems to be able to learn both semantic concepts shared across instances in the same category and instance specific features. For instance, in the bottom-right example of a bird class, one attention head focuses on the black bird only, while the other attend to both birds in the image. More examples are shown in Appendix C.

4.2 Object detection on COCO

Dataset: We evaluate the object detection performance of our SOFT on the COCO benchmark [23] including the train2017 (118k images) and val2017 (5k images) sets.

Implementation details: We consider the following mainstream detectors: RetinaNet [44], Mask R-CNN [45], Cascade Mask R-CNN [51], ATSS [52], GFL [53], Sparse R-CNN [54]. We use AdamW optimizer with base learning rate of 1×10^{-4} and weight decay of 0.01. We train all the model with batch size 16 on 8 V100 GPUs. Following the practices of MMDetection [55], we adopt the 1× and 3× training schedules. In the training stage without multi-scale, images are resized to make the shorter sides at 800 pixels and the longer sides no exceeding 1333 pixels. In the training stage with multi-scale, the shorter sides of images are randomly resized between 480 to 800.

Comparison with state-of-the-art CNNs and ViTs: We compare with the state-of-the-art alternatives on RetinaNet [44] and Mask R-CNN [45] in Table 4. Our SOFT outperforms the CNN ResNet [3] and Transformer counterparts PVT [4] across all complexity groups in both object detection and instance segmentation.

Comparison with different detectors: Table 5 compares the results of SOFT and ResNet50 [3] across four different object detection designs. It is shown that SOFT holds at least +2% box AP gain over ResNet50 with similar parameters and FLOPs.

TABLE 5

Comparison with different object detection designs. “Cascade” stands for Cascade Mask R-CNN and “sparse” stands for sparse R-CNN. AP^b represents bounding box AP.

Backbone	Method	AP ^b	Params	FLOPs
ResNet50 [3]	Cascade [51]	46.3	77M	394G
SOFT-Small		48.3	77M	399G
ResNet50 [3]	ATSS [52]	43.5	32M	205G
SOFT-Small		46.7	32M	215G
ResNet50 [3]	GFL [53]	44.5	32M	208G
SOFT-Small		46.7	32M	219G
ResNet50 [3]	Sparse [54]	44.5	106M	166G
SOFT-Small		47.1	106M	178G

4.3 Semantic segmentation on ADE20K

Dataset: We evaluate the semantic segmentation performance of our SOFT on the ADE20K benchmark [24] with 150 categories and 25k images in total (20k/2k/3k for training/validation/testing).

Implementation details: UperNet [56] is used as the framework. AdamW optimizer with 6×10^{-4} learning rate is applied to train for 160k iterations. Multi-scale training and test time augmentation are not used.

Comparison with state-of-the-art CNNs and ViTs: Table 6 shows that SOFT surpasses ResNet clearly, and the newest designed vision transformer Twins [8] and Swin [41] slightly under the similar parameters and float point computation cost.

TABLE 6

Semantic segmentation on the ADE20k validation set.

Backbone	UperNet		
	Params	FLOPs	mIoU
ResNet50 [3]	67M	238G	42.1
Swin-T [41]	60M	241G	45.8
Twins-PCPVT-S [8]	54M	232G	46.0
SOFT-Small	54M	233G	46.2
ResNet101 [3]	86M	257G	43.8
Swin-S [41]	81M	264G	47.7
Twins-PCPVT-B [41]	75M	253G	47.9
SOFT-Medium	76M	254G	48.0

4.4 Ablation studies

Pyramidal architecture: Unlike the earlier non-pyramidal vision Transformers (*e.g.*, ViT [6]), most recent pyramidal (multi-scale) Transformers (*e.g.*, PVT [4]) use convolution layers to reduce the spatial resolution (*i.e.*, token sequence length) between stages. In this study, we ablate SOFT with a pyramidal architecture (our default SOFT-Small), SOFT w/o a pyramidal architecture and DeiT-S [5] (no pyramidal architecture either). We replace the Transformer layer with a SOFT layer to get SOFT w/o a pyramidal architecture. Note all three variants have similar parameters and FLOPs. Table 9a shows that the conv-based pyramidal architecture is clearly superior to a non-pyramidal design, and our non-pyramidal counterpart is even slightly better than DeiT-S [5] whilst enjoying linear complexity.

Bottleneck token sequence length: In this study, we examine how the bottleneck token sequence length m , sampled from n tokens, influences the model’s performance. We change the bottleneck token sequence length in all stages to 36, 49, 64, 81. Table 7 shows that longer bottleneck token would increase the memory cost and

TABLE 7
Ablations on bottleneck token sequence length.

Bottleneck	Memory	FLOPs	Top-1 %
36	15.1GB	1.9G	79.0
49	15.8GB	1.9G	79.4
64	16.9GB	2.0G	79.4
81	18.5GB	2.1G	78.9

TABLE 8
Ablations on sampling methods.

Sampling methods	Params	FLOPs	Top-1 %
Convolution	13.07M	2.0G	79.4
Random sampling	12.96M	1.9G	79.3
Biased sampling	12.96M	1.9G	79.0
Average pooling	12.96M	1.9G	79.3

the computational overhead. $m = 49$ seems to give the best trade-off between the performance and computational overhead. The memory usage is measured with the batch size of 128.

TABLE 9

(a) Ablations on pyramidal architecture. “Pyr.” stands for the word pyramidal. (b) Ablations on overlapped convolution. “O.L.” stands for the word overlapped

Methods	Pyr.?	Top-1 %	Methods	O.L.?	Top-1 %
DeiT-S [5]	✗	79.8	PVT [4]	✗	75.1
SOFT	✗	80.1	SOFT	✗	77.4
SOFT	✓	82.4	SOFT	✓	79.4

Token sampling: The sampling function in SOFT can assume different forms. **Convolution:** The sequence $Q \in \mathbb{R}^{n \times d_e}$ is first reshaped to a feature map $\mathbb{R}^{H \times W \times d_e}$. $r \times r$ convolution kernel with stride of r is applied for downsampling, where $r = \sqrt{sp}$. The output channel size is also kept and no bias is used. At last, the feature map is reshaped back to the sequence. **Average pooling:** using a $r \times r$ kernel and r stride, where $r = \sqrt{sp}$. **Random sampling:** m tokens are randomly picked from n tokens. **Biased sampling:** We pick m tokens with a biased policy. Here, the first m tokens are picked. Table 8 shows that both convolution yields the best performance. Biased sampling can miss the most salient samples, and there is no guarantee that random sampling can keep the uniformity of the chosen samples. This result thus justifies the choice of using convolution in SOFT.

Overlapped convolution: We ablate SOFT with overlapped convolution (our default choice, same as many recent works) and SOFT with non-overlapped convolution in our Tiny configuration. Table 9b shows that SOFT with overlapped convolution performs better than SOFT without overlapped convolution. Our non-overlapped convolution variant still outperforms the PVT [4] which also has the same non-overlapped convolution by a clear margin.

Newton-Raphson’s convergence: We study how many iterations the Newton-Raphson method needs to converge when computing the Moore-Penrose inverse A^\dagger . We use $\|AA_kA - A\|_p / \|A\|_p$ with $p = 2$ (see Proposition 2) as the convergence metric to quantify the difference between A_k and A^\dagger . Figure 4 shows that our approximation converges within 20 iterations across all stages in all three datasets.

Attention normalization Model generalizability is concerned with transfer learning ability [58], [59]. To more explicitly measure this

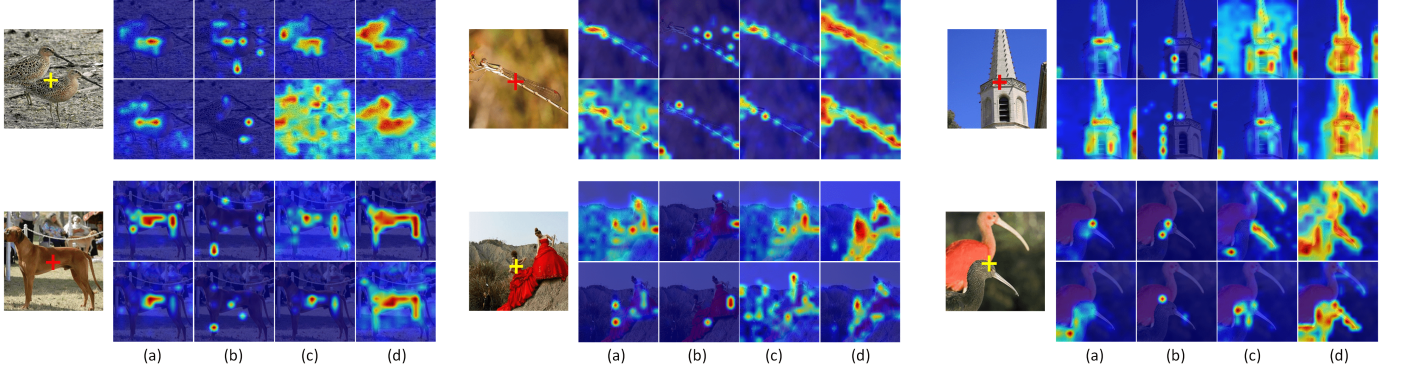


Fig. 3. Comparing the attention heatmaps of a query patch (marked by a cross "+") against all the patches of an image, produced by (a) Transformer [10], (b) Performer [13], (c) Nystromformer [12] and (d) Our SOFT. See Appendix C for more examples.

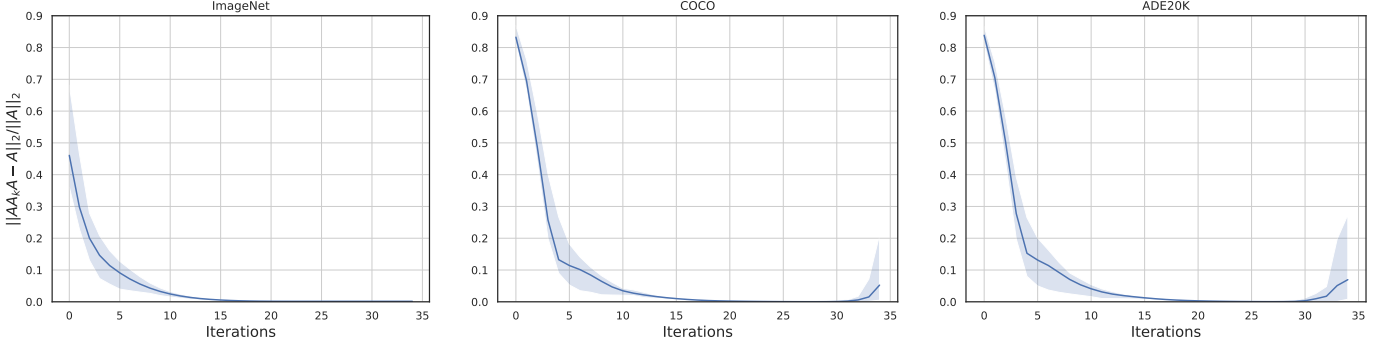


Fig. 4. Convergence analysis for the approximation of Moore-Penrose inverse on ImageNet, COCO and ADE20K separately. SOFT-Tiny is used. We measure $\|AA_k A - A\|_p / \|A\|_2$ for 100 input images on each dataset. The solid line shows the average convergence metric, while the shallow area indicates the upper bound and lower bound.

TABLE 10

Evaluating the effect of the proposed Attention Normalization (A.N.) on downstream tasks including object detection on COCO and semantic segmentation on ADE20K. SOFT-small pretrained on ImageNet is used.

We report *one-epoch fine-tuning* performance. “Pretraining” column gives Top-1 classification accuracy on ImageNet.

A.N.?	Pretraining	RetinaNet	Mask R-CNN	UperNet
	Top-1 %	mAP ^b on COCO	mIoU on ADE20K	
✗	82.4	2.3	1.7	10.7
✓	82.4	28.5	30.30	39.5

capability, we consider the *one-epoch fine-tuning* performance on downstream tasks including object detection on COCO and semantic segmentation on ADE20K. With SOFT-small as the backbone, we test RetinaNet [44], Mask R-CNN [45] and UperNet [56]. As shown in Table 10, although making no difference for ImageNet classification, attention normalization improves both object detection and segmentation significantly. This is because the leading eigenvalue of Gaussian kernel self-attention is conditioned on the token sequence length (Proposition 4), as shown in Figure 5a. This can be clearly mitigated by our normalization scheme (Figure 5b).

4.5 Additional experiments on NLP tasks

In this section, we evaluate our method against other linear counterparts on four tasks of the Long Range Arena (LRA) [57] benchmark *e.g.*, Listops [60], byte-level IMDb reviews text

classification [61], byte-level document retrieval [62], and image classification on sequences of pixels [63].

Implementations. We use the Pytorch version of LRA [57] benchmark, provided by [12]. For the evaluation protocol, we strictly follow [12], [57]. We omit the Pathfinder(1K) task as we cannot replicate the result of Nyströmformer [12]. For our SOFT, we simply use the average pooling with window size 4, stride 4 to sample the bottlenecks. We follow the configurations of [12] with 2 layers, 64 and 128 hidden dimension respectively, and 2 attention heads. The results in Table 11 shows that our SOFT outperforms both the standard and alternative efficient Transformers on three out of four tasks, as well as the average performance.

5 CONCLUSIONS

In this work, we have introduced a novel softmax-free self-attention (SOFT) mechanism for linearizing Transformer’s complexity in space and time. Unlike existing linear Transformers that aim to approximate the conventional softmax based self-attention, SOFT employs a Gaussian kernel based attention which eliminates the need for softmax normalization. This design enables a full self-attention matrix to be approximated via low-rank matrix decomposition. The robustness of this proposed approximation is achieved by calculating its Moore-Penrose inverse using a Newton-Raphson method and an efficient symmetric attention normalization. Extensive experiments show that SOFT yields superior trade-off in accuracy and complexity on a variety of vision and language tasks.

TABLE 11

Comparison of different linear/efficient Transformer variants on Long Range Arena [57], based on its official configuration. Our SOFT surpasses previous efficient methods on three tasks.

Methods	Listops(2K)	Text(4K)	Retrieval(4K)	Image(1K)	Avg. %
Transformer [10]	37.10	65.02	79.35	38.20	54.92
Reformer [20]	19.05	64.88	78.64	43.29	51.47
Linformer [11]	37.25	55.91	79.37	37.84	52.59
Performer [13]	18.80	63.81	78.62	37.07	49.58
Nyströmformer [12]	37.15	65.52	79.56	41.58	55.95
SOFT	37.40	63.49	81.77	46.91	57.39

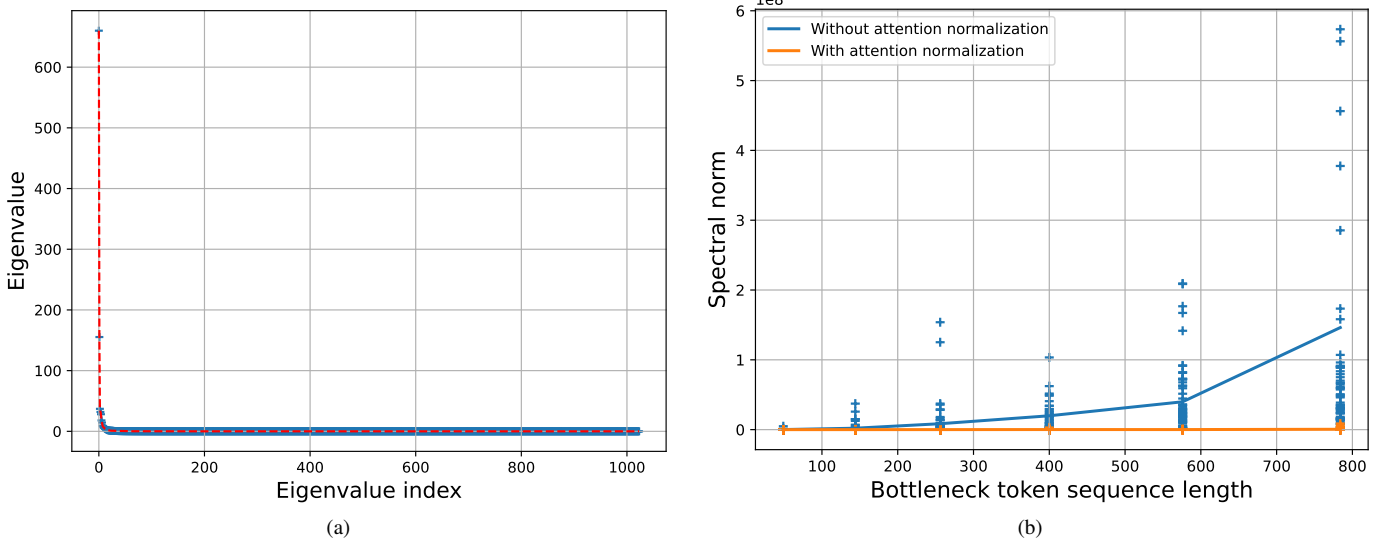


Fig. 5. (a) Eigenvalues of a specific bottleneck matrix $A \in \mathbb{R}^{1024 \times 1024}$. The auxiliary (red dash) line connects all the eigenvalues. (b) Comparing the spectral norm of self-attention matrix A^{\dagger} (without normalization, blue) and $D^{-1/2}A^{\dagger}D^{-1/2}$ (with normalization, orange) under a variety of bottleneck token sequence lengths. "+" represent individual samples; The lines connect the average norm at each token sequence length.

APPENDIX A NYSTRÖM METHOD

Nyström method [31] aims to calculate a low-rank approximation for a Gram matrix. For Transformers, the self-attention matrix can be viewed as a Gram matrix S with a Gaussian kernel k applied to the query Q , with each element S_{ij} expressed as:

$$S_{ij} = k(Q_{i,:}, Q_{j,:}) = \exp\left(-\frac{\|Q_{i,:} - Q_{j,:}\|_2^2}{2\sqrt{d}}\right), \quad (26)$$

$k(x, y)$ means operating Gaussian kernel k to (x, y) , which can be written in the feature space as:

$$k(x, y) = \sum_{i=1}^n \lambda_i \phi_i(x) \phi_i(y), \quad (27)$$

n is the dimension of a feature space, λ_i denotes the eigenvalue and ϕ_i denotes the eigenfunction of kernel k . According to the eigenfunction's definition, we can get:

$$\int k(y, x) \phi_i(x) p(x) dx = \lambda_i \phi_i(y), \quad (28)$$

where $p(x)$ is the probability distribution of x . And $\{\phi_i(x)\}$ are p -orthogonal:

$$\int \phi_i(x) \phi_j(x) p(x) dx = \delta_{ij}. \quad (29)$$

δ_{ij} is 0 when $i \neq j$, 1 when $i = j$. To get an approximation of the eigenfunctions, we sample $\{x_1, x_2, \dots, x_q\}$ from $p(x)$, then:

$$\frac{1}{q} \sum_{t=1}^q k(y, x_t) \phi_i(x_t) \approx \lambda_i \phi_i(y), \quad (30)$$

$$\frac{1}{q} \sum_{t=1}^q \phi_i(x_t) \phi_j(x_t) \approx \delta_{ij}. \quad (31)$$

This inspires us to approximate the Gram matrix S . Let $S^{(m)}$ be a submatrix of S , consisting of $m \times m$ elements from S . Gram matrix is a symmetric positive semi-definite matrix, so it has a spectral decomposition:

$$S^{(m)} U^{(m)} = U^{(m)} \Lambda^{(m)}, \quad (32)$$

where $U^{(m)}$ is column orthogonal and $\Lambda^{(m)}$ is a diagonal matrix with the diagonal elements as the eigenvalues of $S^{(m)}$. Substituting the y to x_j and applying the approximation above to S , we can get:

$$\phi_i(x_j) \approx \sqrt{m} U_{j,i}^{(m)}, \quad \lambda_i \approx \frac{\lambda_i^{(m)}}{m}, \quad (33)$$

$$\phi_i(y) \approx \frac{\sqrt{m}}{\lambda_i^{(m)}} \sum_{t=1}^m k(y, x_t) \phi_i(x_t), \quad (34)$$

λ_i is eigenvalue of S and $\lambda_i^{(m)}$ is the eigenvalue of $S^{(m)}$. Denote \tilde{S} as the rank- m approximation of S and $\tilde{U}, \tilde{\Lambda}$ as the approximation for spectral decomposition of S . Now we can get an approximation of S with rank m :

$$\tilde{S} = \tilde{U} \tilde{\Lambda} \tilde{U}^T = \sum_{t=1}^m \tilde{\lambda}_t^{(n)} \tilde{u}_t^{(n)} (\tilde{u}_t^{(n)})^T. \quad (35)$$

Similarly, we have:

$$\phi_i(x_j) \approx \sqrt{n} U_{j,i}(n), \quad \lambda_i \approx \frac{\tilde{\lambda}_i^{(n)}}{n}. \quad (36)$$

Thus

$$\tilde{\lambda}_i^{(n)} \approx \frac{n \lambda_i^{(m)}}{m}, \quad (37)$$

$$\tilde{u}_t^{(n)} \approx \sqrt{\frac{m}{n}} \frac{1}{\lambda_t^{(m)}} S_{n,m} u_t^{(m)}. \quad (38)$$

Then we get an approximation of S : $\tilde{S} \approx S_{n,m} S_{m,m}^\dagger S_{m,n} \cdot S$ has a block representation below:

$$S = \begin{bmatrix} S_{m,m} & S_{m,n-m} \\ S_{n-m,m} & S_{n-m,n-m} \end{bmatrix}. \quad (39)$$

APPENDIX B

NON-LINEARIZED GAUSSIAN KERNEL ATTENTION

Instead of directly calculating the Gaussian kernel weights, in our formulation they are approximated. More specifically, the relation between any two tokens is reconstructed via sampled bottleneck tokens. As the number m (e.g., 49) of bottleneck tokens is much smaller than the entire token sequence length, our attention matrix is of low-rank. This brings about two favorable consequences: **(I)** The model now focuses the attentive learning on latent salient information captured by the m bottleneck tokens. **(II)** The model becomes more robust against the underlying token noise due to the auto-encoder style reconstruction [64].

This explains why a model with an approximated gram matrix performs better than one with a directly computed matrix. Further, we find that exact Gaussian kernel attention leads to training difficulties. As Proposition 4 reveals, this is due to lacking normalization that leads to explosion of the spectral norm especially in long token sequence cases. Big spectral norm could jeopardize the training and tend to collapse the model.

APPENDIX C

ATTENTION VISUALIZATION

Figure 6 shows more visualization of the attention masks by various Transformers [10], [12], [13] and our SOFT. For each model, we show the output from the first two attention heads (up and down row). It is noteworthy that SOFT exhibits better semantic diversity of the multi-head mechanism than other methods. Moreover, when we sample the patch at the boundary of multiple objects, SOFT is able to more precisely capture all these objects.

ACKNOWLEDGMENTS

We thank Jinghan Yao, Weiguo Gao, Chunjing Xu and Tao Xiang for valuable discussions. This work was supported in part by National Natural Science Foundation of China (Grant No. 6210020439), Lingang Laboratory (Grant No. LG-QS-202202-07) and Natural Science Foundation of Shanghai (Grant No. 22ZR1407500).

REFERENCES

- [1] J. Deng, W. Dong, R. Socher, L.-J. Li, K. Li, and L. Fei-Fei, “Imagenet: A large-scale hierarchical image database,” in *IEEE Conference on Computer Vision and Pattern Recognition*, 2009. [2](#), [6](#), [7](#), [8](#)
- [2] I. Radosavovic, R. P. Kosaraju, R. Girshick, K. He, and P. Dollár, “Designing network design spaces,” in *IEEE Conference on Computer Vision and Pattern Recognition*, 2020. [2](#), [8](#)
- [3] K. He, X. Zhang, S. Ren, and J. Sun, “Deep residual learning for image recognition,” in *IEEE Conference on Computer Vision and Pattern Recognition*, 2016. [2](#), [7](#), [8](#), [9](#)
- [4] W. Wang, E. Xie, X. Li, D.-P. Fan, K. Song, D. Liang, T. Lu, P. Luo, and L. Shao, “Pyramid vision transformer: A versatile backbone for dense prediction without convolutions,” *arXiv preprint*, 2021. [2](#), [6](#), [7](#), [8](#), [9](#)
- [5] H. Touvron, M. Cord, M. Douze, F. Massa, A. Sablayrolles, and H. Jégou, “Training data-efficient image transformers & distillation through attention,” *arXiv preprint*, 2020. [2](#), [7](#), [8](#), [9](#)
- [6] A. Dosovitskiy, L. Beyer, A. Kolesnikov, D. Weissenborn, X. Zhai, T. Unterthiner, M. Dehghani, M. Minderer, G. Heigold, S. Gelly *et al.*, “An image is worth 16x16 words: Transformers for image recognition at scale,” in *International Conference on Learning Representations*, 2021. [1](#), [2](#), [6](#), [7](#), [8](#), [9](#)
- [7] L. Yuan, Y. Chen, T. Wang, W. Yu, Y. Shi, Z. Jiang, F. E. Tay, J. Feng, and S. Yan, “Tokens-to-token vit: Training vision transformers from scratch on imagenet,” *arXiv preprint*, 2021. [1](#), [2](#), [7](#)
- [8] X. Chu, Z. Tian, Y. Wang, B. Zhang, H. Ren, X. Wei, H. Xia, and C. Shen, “Twins: Revisiting the design of spatial attention in vision transformers,” *arXiv preprint*, 2021. [2](#), [7](#), [8](#), [9](#)
- [9] H. Zhao, J. Jia, and V. Koltun, “Exploring self-attention for image recognition,” in *IEEE Conference on Computer Vision and Pattern Recognition*, 2020. [2](#)
- [10] A. Vaswani, N. Shazeer, N. Parmar, J. Uszkoreit, L. Jones, A. N. Gomez, L. Kaiser, and I. Polosukhin, “Attention is all you need,” in *Advances in Neural Information Processing Systems*, 2017. [1](#), [2](#), [3](#), [6](#), [10](#), [11](#), [12](#), [13](#)
- [11] S. Wang, B. Li, M. Khabsa, H. Fang, and H. Ma, “Linformer: Self-attention with linear complexity,” *arXiv preprint*, 2020. [1](#), [2](#), [6](#), [7](#), [8](#), [11](#)
- [12] Y. Xiong, Z. Zeng, R. Chakraborty, M. Tan, G. Fung, Y. Li, and V. Singh, “Nyströmformer: A nyström-based algorithm for approximating self-attention,” in *AAAI Conference on Artificial Intelligence*, 2021. [1](#), [2](#), [3](#), [6](#), [7](#), [8](#), [10](#), [11](#), [12](#), [13](#)
- [13] K. Choromanski, V. Likhoshesterov, D. Dohan, X. Song, A. Gane, T. Sarlos, P. Hawkins, J. Davis, A. Mohiuddin, L. Kaiser *et al.*, “Rethinking attention with performers,” in *International Conference on Learning Representations*, 2021. [1](#), [2](#), [6](#), [7](#), [8](#), [10](#), [11](#), [12](#), [13](#)
- [14] J. Devlin, M.-W. Chang, K. Lee, and K. Toutanova, “Bert: Pre-training of deep bidirectional transformers for language understanding,” in *ACL*, 2018. [1](#), [2](#)
- [15] T. B. Brown, B. Mann, N. Ryder, M. Subbiah, J. Kaplan, P. Dhariwal, A. Neelakantan, P. Shyam, G. Sastry, A. Askell *et al.*, “Language models are few-shot learners,” in *Advances in Neural Information Processing Systems*, 2020. [1](#), [2](#)
- [16] X. Zhu, W. Su, L. Lu, B. Li, X. Wang, and J. Dai, “Deformable detr: Deformable transformers for end-to-end object detection,” in *International Conference on Learning Representations*, 2021. [1](#)
- [17] S. Zheng, J. Lu, H. Zhao, X. Zhu, Z. Luo, Y. Wang, Y. Fu, J. Feng, T. Xiang, P. H. Torr, and L. Zhang, “Rethinking semantic segmentation from a sequence-to-sequence perspective with transformers,” in *IEEE Conference on Computer Vision and Pattern Recognition*, 2021. [1](#)
- [18] S. d’Ascoli, H. Touvron, M. Leavitt, A. Morcos, G. Biroli, and L. Sagun, “Convit: Improving vision transformers with soft convolutional inductive biases,” in *International Conference on Machine Learning*, 2021. [1](#)
- [19] A. Jaegle, F. Gimeno, A. Brock, A. Zisserman, O. Vinyals, and J. Carreira, “Perceiver: General perception with iterative attention,” *arXiv preprint*, 2021. [1](#)
- [20] N. Kitayev, L. Kaiser, and A. Levskaya, “Reformer: The efficient transformer,” in *International Conference on Learning Representations*, 2020. [1](#), [2](#), [8](#), [11](#)
- [21] A. Katharopoulos, A. Vyas, N. Pappas, and F. Fleuret, “Transformers are rnns: Fast autoregressive transformers with linear attention,” in *International Conference on Machine Learning*, 2020. [1](#), [2](#)
- [22] J. Lu, J. Yao, J. Zhang, X. Zhu, H. Xu, W. Gao, C. Xu, T. Xiang, and L. Zhang, “Soft: softmax-free transformer with linear complexity,” *Advances in Neural Information Processing Systems*, 2021. [2](#)
- [23] T.-Y. Lin, M. Maire, S. Belongie, J. Hays, P. Perona, D. Ramanan, P. Dollár, and C. L. Zitnick, “Microsoft coco: Common objects in context,” in *European Conference on Computer Vision*, 2014. [2](#), [8](#)

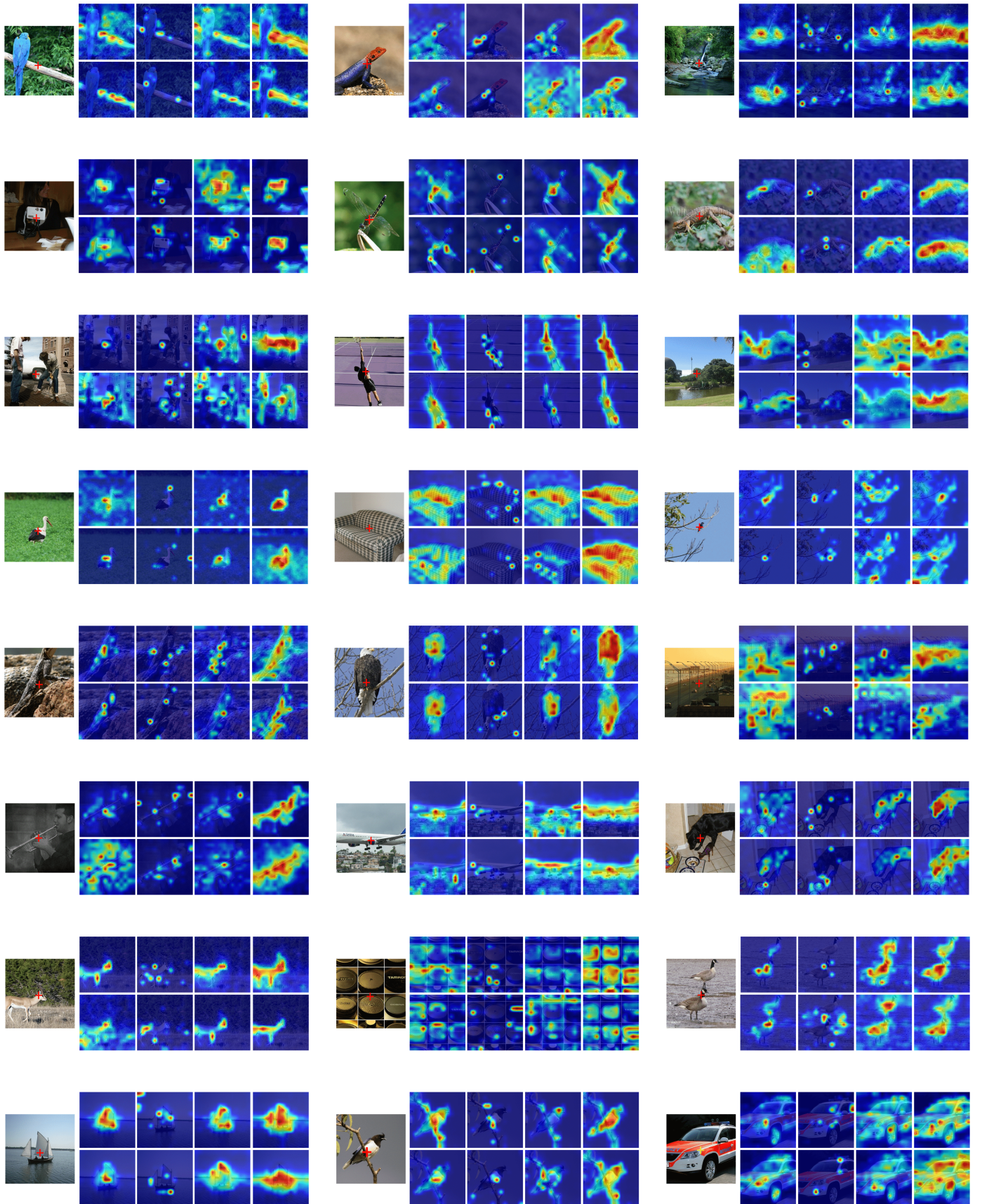


Fig. 6. Comparing the attention heatmaps of a query patch (marked by the cross "+") against all the patches of an image, produced by (a) Transformer [10], (b) Performer [13], (c) Nyströmformer [12] and (d) SOFT (Ours).

[24] B. Zhou, H. Zhao, X. Puig, T. Xiao, S. Fidler, A. Barriuso, and A. Torralba, “Semantic understanding of scenes through the ade20k dataset,” *International Journal of Computer Vision*, 2019. [2](#) [9](#)

[25] X. Wang, R. Girshick, A. Gupta, and K. He, “Non-local neural networks,” in *IEEE Conference on Computer Vision and Pattern Recognition*, 2018. [2](#)

[26] L. Zhang, D. Xu, A. Arnab, and P. H. Torr, “Dynamic graph message passing networks,” in *IEEE Conference on Computer Vision and Pattern Recognition*, 2020. [2](#)

[27] Y. Tay, M. Dehghani, D. Bahri, and D. Metzler, “Efficient transformers: A survey,” *arXiv preprint*, 2020. [2](#)

[28] H. Peng, N. Pappas, D. Yogatama, R. Schwartz, N. A. Smith, and L. Kong, “Random feature attention,” *arXiv preprint arXiv:2103.02143*, 2021. [2](#)

[29] J. Kasai, H. Peng, Y. Zhang, D. Yogatama, G. Ilharco, N. Pappas, Y. Mao, W. Chen, and N. A. Smith, “Finetuning pretrained transformers into rnns,” *arXiv preprint arXiv:2103.13076*, 2021. [2](#)

[30] G. E. Fasshauer, “Positive definite kernels: past, present and future,” *Dolomites Research Notes on Approximation*, 2011. [3](#)

[31] C. Williams and M. Seeger, “Using the nyström method to speed up kernel machines,” in *Advances in Neural Information Processing Systems*, 2001. [3](#) [11](#)

[32] A. Ben-Israel and D. Cohen, “On iterative computation of generalized inverses and associated projections,” *SIAM Journal on Numerical Analysis*, 1966. [4](#)

[33] Y. Yoshida and T. Miyato, “Spectral norm regularization for improving the generalizability of deep learning,” *arXiv preprint*, 2017. [5](#)

[34] U. Von Luxburg, “A tutorial on spectral clustering,” *Statistics and computing*, 2007. [5](#)

[35] J. Cheng, M. Grossman, and T. McKercher, *Professional CUDA c programming*. John Wiley & Sons, 2014. [6](#)

[36] J. L. Ba, J. R. Kiros, and G. E. Hinton, “Layer normalization,” *arXiv preprint*, 2016. [6](#)

[37] S. Ioffe and C. Szegedy, “Batch normalization: Accelerating deep network training by reducing internal covariate shift,” in *International Conference on Machine Learning*, 2015. [6](#)

[38] W. Xu, Y. Xu, T. Chang, and Z. Tu, “Co-scale conv-attentional image transformers,” *arXiv preprint*, 2021. [7](#)

[39] I. Bello, “Lambdanetworks: Modeling long-range interactions without attention,” *arXiv preprint*, 2021. [7](#)

[40] X. Chu, Z. Tian, B. Zhang, X. Wang, X. Wei, H. Xia, and C. Shen, “Conditional positional encodings for vision transformers,” *arXiv preprint*, 2021. [7](#)

[41] Z. Liu, Y. Lin, Y. Cao, H. Hu, Y. Wei, Z. Zhang, S. Lin, and B. Guo, “Swin transformer: Hierarchical vision transformer using shifted windows,” in *IEEE International Conference on Computer Vision*, 2021. [7](#) [8](#) [9](#)

[42] A. Srinivas, T.-Y. Lin, N. Parmar, J. Shlens, P. Abbeel, and A. Vaswani, “Bottleneck transformers for visual recognition,” *arXiv preprint*, 2021. [7](#)

[43] H. Touvron, M. Cord, A. Sablayrolles, G. Synnaeve, and H. Jégou, “Going deeper with image transformers,” *arXiv preprint*, 2021. [7](#)

[44] T.-Y. Lin, P. Goyal, R. Girshick, K. He, and P. Dollár, “Focal loss for dense object detection,” in *IEEE International Conference on Computer Vision*, 2017. [8](#) [10](#)

[45] K. He, G. Gkioxari, P. Dollár, and R. Girshick, “Mask r-cnn,” in *IEEE International Conference on Computer Vision*, 2017. [8](#) [10](#)

[46] R. Wightman, “Pytorch image models,” <https://github.com/rwightman/pytorch-image-models>, 2019. [6](#)

[47] H. Zhang, M. Cisse, Y. N. Dauphin, and D. Lopez-Paz, “mixup: Beyond empirical risk minimization,” *arXiv preprint*, 2017. [7](#)

[48] S. Yun, D. Han, S. J. Oh, S. Chun, J. Choe, and Y. Yoo, “Cutmix: Regularization strategy to train strong classifiers with localizable features,” in *IEEE International Conference on Computer Vision*, 2019. [7](#)

[49] C. Szegedy, V. Vanhoucke, S. Ioffe, J. Shlens, and Z. Wojna, “Rethinking the inception architecture for computer vision,” in *IEEE Conference on Computer Vision and Pattern Recognition*, 2016. [7](#)

[50] Mindspore, “<https://www.mindspore.cn/>,” 2020. [7](#)

[51] Z. Cai and N. Vasconcelos, “Cascade r-cnn: high quality object detection and instance segmentation,” *IEEE Transactions on Pattern Analysis and Machine Intelligence*, 2019. [8](#) [9](#)

[52] S. Zhang, C. Chi, Y. Yao, Z. Lei, and S. Z. Li, “Bridging the gap between anchor-based and anchor-free detection via adaptive training sample selection,” in *IEEE Conference on Computer Vision and Pattern Recognition*, 2020. [8](#) [9](#)

[53] X. Li, W. Wang, L. Wu, S. Chen, X. Hu, J. Li, J. Tang, and J. Yang, “Generalized focal loss: Learning qualified and distributed bounding boxes for dense object detection,” *Advances in Neural Information Processing Systems*, 2020. [8](#) [9](#)

[54] P. Sun, R. Zhang, Y. Jiang, T. Kong, C. Xu, W. Zhan, M. Tomizuka, L. Li, Z. Yuan, C. Wang *et al.*, “Sparse r-cnn: End-to-end object detection with learnable proposals,” in *IEEE Conference on Computer Vision and Pattern Recognition*, 2021. [8](#) [9](#)

[55] K. Chen, J. Wang, J. Pang, Y. Cao, Y. Xiong, X. Li, S. Sun, W. Feng, Z. Liu, J. Xu *et al.*, “Mmdetection: Open mmlab detection toolbox and benchmark,” *arXiv preprint*, 2019. [8](#)

[56] T. Xiao, Y. Liu, B. Zhou, Y. Jiang, and J. Sun, “Unified perceptual parsing for scene understanding,” in *European Conference on Computer Vision*, 2018. [9](#) [10](#)

[57] Y. Tay, M. Dehghani, S. Abnar, Y. Shen, D. Bahri, P. Pham, J. Rao, L. Yang, S. Ruder, and D. Metzler, “Long range arena: A benchmark for efficient transformers,” *arXiv preprint*, 2020. [10](#) [11](#)

[58] J. Wang, C. Lan, C. Liu, Y. Ouyang, T. Qin, W. Lu, Y. Chen, W. Zeng, and P. Yu, “Generalizing to unseen domains: A survey on domain generalization,” *IEEE Transactions on Knowledge and Data Engineering*, 2022. [9](#)

[59] S. Akhauri, L. Zheng, T. Goldstein, and M. Lin, “Improving generalization of transfer learning across domains using spatio-temporal features in autonomous driving,” *arXiv preprint*, 2021. [9](#)

[60] N. Nangia and S. R. Bowman, “Listops: A diagnostic dataset for latent tree learning,” *arXiv preprint*, 2018. [10](#)

[61] A. Maas, R. E. Daly, P. T. Pham, D. Huang, A. Y. Ng, and C. Potts, “Learning word vectors for sentiment analysis,” in *Proceedings of the 49th annual meeting of the association for computational linguistics: Human language technologies*, 2011. [10](#)

[62] D. R. Radev, P. Muthukrishnan, V. Qazvinian, and A. Abu-Jbara, “The acl anthology network corpus,” *Language Resources and Evaluation*, 2013. [10](#)

[63] A. Krizhevsky, G. Hinton *et al.*, “Learning multiple layers of features from tiny images,” *Citeseer*, 2009. [10](#)

[64] Z. Geng, M.-H. Guo, H. Chen, X. Li, K. Wei, and Z. Lin, “Is attention better than matrix decomposition?” in *International Conference on Learning Representations*, 2021. [12](#)